Available online at www.sciencedirect.com
SCIENCE DIRECT
ELSEVIER
Nuclear Instruments and Methods in Physics Research A 541 (2005) 357–364
NUCLEAR INSTRUMENTS & METHODS IN PHYSICS RESEARCH Section A
www.elsevier.com/locate/nima

X-ray imaging spectrometers (XIS) of Astro-E2

H. Matsumoto[a,*], K. Koyama[a], T.G. Tsuru[a], H. Nakajima[a], H. Yamaguchi[a], H. Tsunemi[b], K. Hayashida[b], E. Miyata[b], K. Torii[b], M. Namiki[b], T. Dotani[c], M. Ozaki[c], H. Murakami[c], N. Anabuki[c], S. Kitamoto[d], H. Awaki[e], T. Kohmura[f], H. Katayama[g], A. Bamba[h], M.W. Bautz[i], J.P. Doty[i], G.R. Ricker[i], R.F. Foster[i], G.Y. Prigozhin[i], S.E. Kissel[i], B.E. Burke[i], A.D. Pillsbury[i], B. LaMarr[i]

[a]*Department of Physics, Faculty of Science, Kyoto University, Kitashirakawa-Oiwake-Cho, Sakyo-ku, Kyoto 606-8502, Japan*
[b]*Department of Earth and Space Science, Graduate School of Science, Osaka University, 1-1 Machikaneyama, Toyonaka, Osaka 560-0043, Japan*
[c]*ISAS/JAXA, 3-1-1 Yoshinodai, Sagamihara, Kanagawa 229-8510, Japan*
[d]*Department of Physics, Rikkyo University, 3-34-1 Nishi-Ikebukro, Toshima-ku, Tokyo 171-8520, Japan*
[e]*Department of Physics, Faculty of Science, Ehime University, Bunkyo-cho, Matsuyama, Ehime 790-8577, Japan*
[f]*Kogakuin University, 2665-1 Nakano-machi, Hachioji, Tokyo 192-0015, Japan*
[g]*JAXA, 2-1-1 Sengen, Tsukuba, Ibaraki 305-8505, Japan*
[h]*RIKEN, 2-1 Hirosawa, Wako, Saitama 351-0198, Japan*
[i]*Center for Space Research, Massachusetts Institute of Technology, 77 Massachusetts Avenue, Cambridge, MA 02139-4307, USA*

Available online 2 March 2005

Abstract

Astro-E2 is the fifth Japanese X-ray astronomical satellite and will be launched in 2005. The Astro-E2 X-ray Imaging Spectrometers (XISs) consist of four sets of X-ray CCD cameras. Each CCD camera has an imaging area of 1024×1024 pixels and covers a region of $18' \times 18'$ on the sky combined with an X-ray Telescope. One XIS will utilize back-side illuminated (BI) CCDs, and the other three will be equipped with front-side illuminated (FI) CCDs. The BI CCD has a higher quantum efficiency than the FI CCD below 2 keV, while the FI CCD is more sensitive to X-rays above 5 keV than the BI CCD. Both types of the CCDs have nearly the same energy resolution (full-width at half-maximum (FWHM) $=\sim 130$ eV at 6 keV). All four cameras have a charge injection capability and ^{55}Fe calibration sources, and we can correct the change of the gain and recover the degradation of the energy resolution due to radiation damage caused

*Corresponding author.
E-mail address: matumoto@cr.scphys.kyoto-u.ac.jp (H. Matsumoto).

doi:10.1016/j.nima.2005.01.076

by cosmic rays. The sensors are cooled to −90 °C to minimize thermal noise in orbit. The low temperature is also helpful to reduce the influence of the radiation damage.

PACS: 95.55.−n; 95.55.Aq; 95.55.Ka

Keywords: X-rays; CCD; Astro-E2

1. Introduction

Astro-E2 is the fifth Japanese X-ray astronomical satellite, which will be launched in 2005. Astro-E2 carries four sets of X-ray charge-coupled device (CCD) cameras, which are referred to as X-ray Imaging Spectrometers (XISs). They are operated in a photon-counting mode similar to the *ASCA* SIS [1], *Chandra* ACIS [2], and *XMM-Newton* EPIC [3].

Two other instruments are also on board Astro-E2: the X-Ray Spectrometer (XRS) [4] and the Hard X-ray Detector (HXD) [5]. The XRS is an X-ray micro-calorimeter with an extremely high energy resolution (full-width at half-maximum (FWHM) 6 eV at 5.9 keV) in the 0.3–12 keV band. The HXD consists of phoswitch scintillation counters (GSO/BGO) and silicon PIN diodes and has a sensitivity in the 10–600 keV band. Only the XIS has an imaging capability with a moderate energy resolution, and is complementary to these detectors. Together these instruments combine to open a new horizon for X-ray astronomy.

The CCD sensors, the analog electronics, and the temperature control electronics of the XIS were developed at MIT; while the digital electronics and a portion of the sensor housing were developed in Japan, jointly by Kyoto University, Osaka University, Rikkyo University, Ehime University, Kogakuin University, and ISAS/JAXA.

2. Overview of the XIS

Fig. 1 gives a schematic view of the XIS system for one sensor. The four XIS sensors (XIS-S0–S3) are located at the foci of four X-ray telescopes (XRT). Each CCD sensor has a single CCD chip, which is a MOS-type three-phase CCD operated in frame transfer mode. The exposure area of the CCD consists of 1024×1024 pixels. The pixel size is $24\,\mu m \times 24\,\mu m$, giving a size of $25\,mm \times 25\,mm$ for the exposure area. The exposure area covers an $18' \times 18'$ region on the sky combined with the XRT.

The CCD sensors are kept at −90 °C to minimize the thermal noise. This is accomplished by thermo-electric coolers (TECs), which are Peltier devices attached to the undersurface of the CCD. The TECs are controlled by TEC control electronics (TCE). The analog electronics (AE) drives the CCD clocks, reads and amplifies the signal from the CCDs, performs the analog-to-digital conversion, and sends the data to the digital electronics (DE). Because the AE and the TCE are in the same housing, they are referred to together as the AE/TCE. There are two AE/TCEs on board Astro-E2: AE/TCE01 is connected to XIS-S0 and S1, and the other AE/TCE23 is used for XIS-S2 and S3. The DE consists of two pixel processing units (PPU01 and PPU23) and one main processing unit (MPU). The PPUs receive the raw data from the AE, and store them into memory which is called Pixel RAM. The PPUs then carry out event detection, and send event data to the MPU. The MPU edits and packets the event data and sends them to the satellite's main digital processor.

Because X-ray CCDs are generally sensitive to optical and UV light, the XIS has an optical blocking filter (OBF) just in front of the imaging area. The OBF is made of a Polyimide ($C_{22}H_{10}N_2O_4$) film over which aluminum is vapor-deposited. The thicknesses of Polyimide and aluminum are 1130 and 1340 Å, respectively.

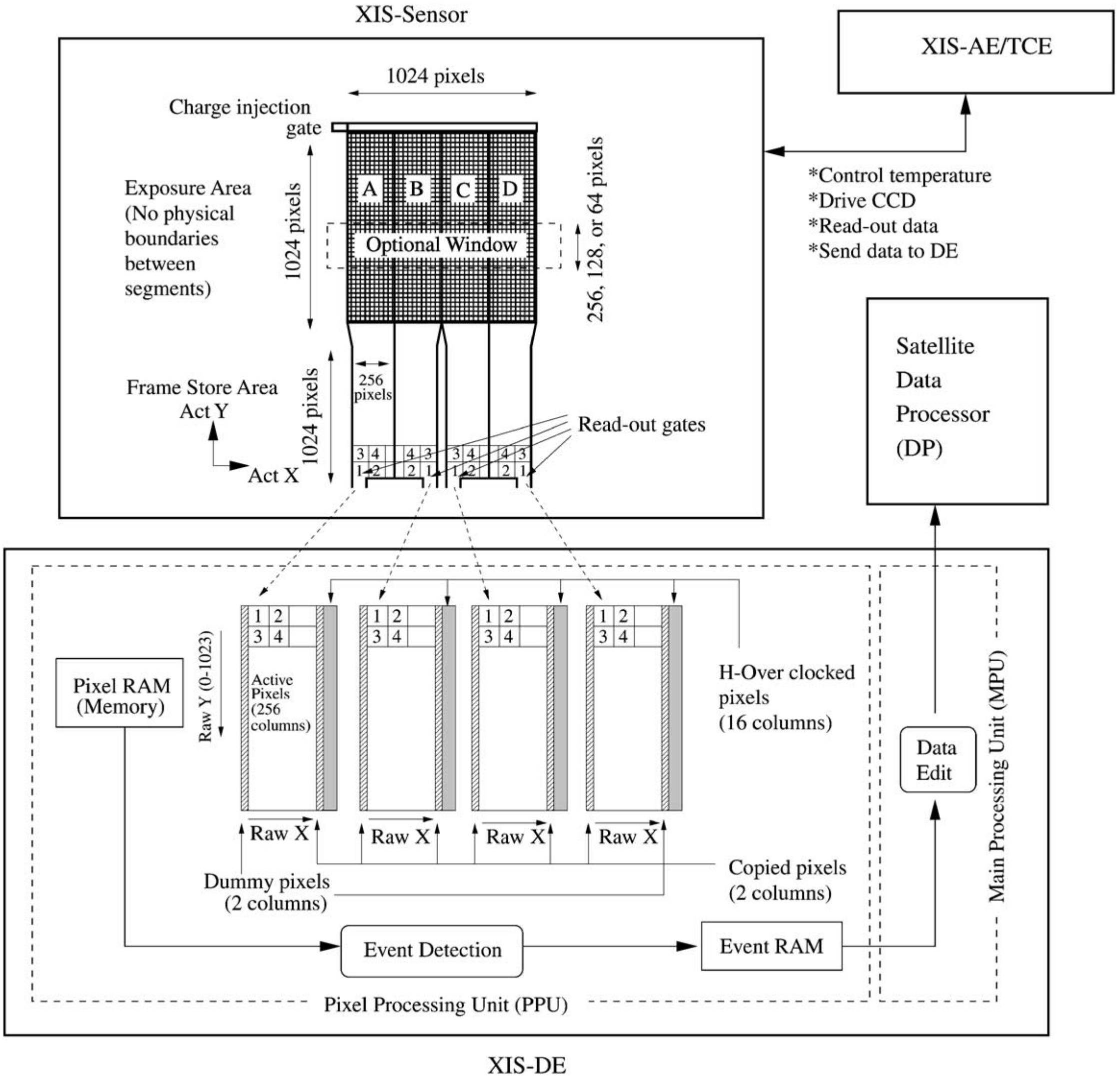

Fig. 1. Schematic view of one XIS system. Each XIS consists of a single CCD chip with an imaging area of 1024×1024 pixels. The pixel size of each pixel of the imaging area is $24\,\mu m \times 24\,\mu m$. Astro-E2 contains four CCD cameras (XIS-S0–S3), two AE/TCEs (AE/TCE01 and AE/TCE23), two PPUs (PPU01 and PPU23), and one MPU. AE/TCE01 and PPU01 are connected to XIS-S0 and XIS-S1, while AE/TCE23 and PPU23 serve XIS-S2 and XIS-S3. One of the four CCDs is back-illuminated (BI), and three are front-illuminated (FI).

The OBF has a low transmission coefficient for optical light ($\leqslant 5 \times 10^{-5}$), while being transparent to X-rays ($\geqslant 80\%$ above 0.7 keV).

For on-orbit calibration, each CCD sensor has three ^{55}Fe calibration sources. One is attached to a door to illuminate the whole imaging area, and the other two are located on the side wall of the housing and illuminate two corners of the imaging area. The door source is used for initial calibration only, and after the door is opened, it will not illuminate the CCD.

The basic characteristics of the XIS are summarized in Table 1. Ground calibrations of the XIS are ongoing. There are some documents in which further information on the XIS is available [6–8].

Table 1
Characteristics of the XIS

Field of view	$18' \times 18'$
Energy range	0.2–12 keV
Imaging area format	1024 × 1024 pixels
Pixel size	24 μm × 24 μm
Energy resolution	~ 130 eV (FWHM) at 6 keV
Effective area[a]	340 cm^2 (FI[b]), 390 cm^2 (BI[c]) at 1.5 keV 150 cm^2 (FI[b]), 100 cm^2 (BI[c]) at 8 keV
Read-out noise	~ 3 electrons (RMS)
Time resolution	8 s (normal mode), 7.8 ms (P-sum mode)

[a]On-axis effective area for one sensor including the OBF transmission, the CCD quantum efficiency, and the XRT effective area. The calculations are for a point source integrated over a circular region with a 6 mm (4.34 arcmin) radius.
[b]Front-illuminated CCD.
[c]Back-illuminated CCD.

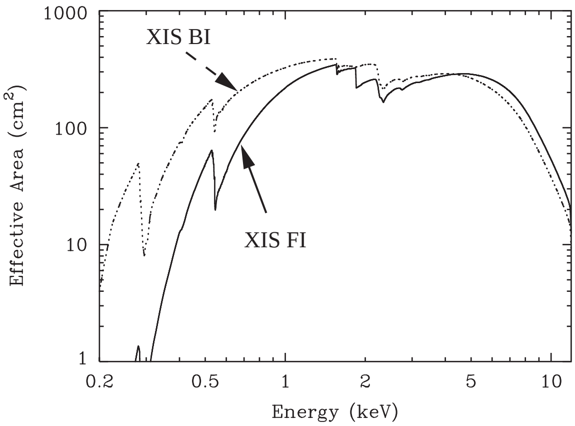

Fig. 2. On-axis effective area for a BI CCD (dotted line) and an FI CCD (thick line) including the OBF transmission, the CCD quantum efficiency, and the XRT effective area. The calculations are for a point source integrated over a circular region with a 6 mm (4.34 arcmin) radius.

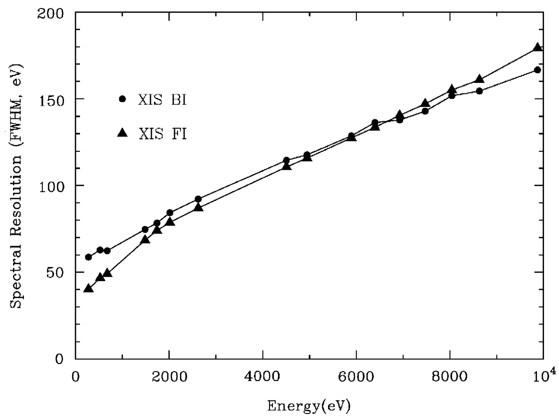

Fig. 3. Energy resolution for the XIS BI (circle) and the XIS FI (triangle).

3. Front-illuminated CCD (FI) and back-illuminated CCD (BI)

There are two types of X-ray CCDs in terms of the incident direction of X-rays: front-side illuminated (FI) CCDs and back-side illuminated (BI) CCDs. In the case of FI CCDs, X-rays reach the CCD through the front surface of the CCD where there is a gate structure which consists mainly of Si and SiO_2, while BI CCDs detect X-rays coming from the back side of the CCD where there is no gate structure. Thus, BI CCDs tend to have a much higher quantum efficiency (QE) for soft X-rays. However, because BI CCDs need to be thinned in order to remove the undepletion layer of BI CCDs completely, the depletion layer of BI CCDs is generally thinner than that of FI CCDs. Therefore the QE of FI CCDs is higher than that of BI CCDs at high energies. One of the four sensors will be equipped with BI CCDs, and the other three will utilize FI CCDs. The effective area of both types of XIS is shown in Fig. 2.

Chandra and *XMM-Newton* also have BI CCDs. The energy resolution of these BI CCDs is worse than that of the FI CCDs. Due to the so-called chemisorption process [9], however, the energy resolution of the XIS BI CCD is significantly improved and is almost the same as that of the XIS FI CCD (Figs. 3 and 4).

4. Clock modes and editing modes

Clock modes specify how to drive the CCD clocks, and an exposure time, exposure region and time resolution are then determined according to the clock modes. Schematic views of the clock modes and options are shown in Fig. 5.

There are two clock modes for the XIS: Normal mode and Parallel-sum (P-sum) mode. In the Normal mode, all pixels are read out. It takes 8 s

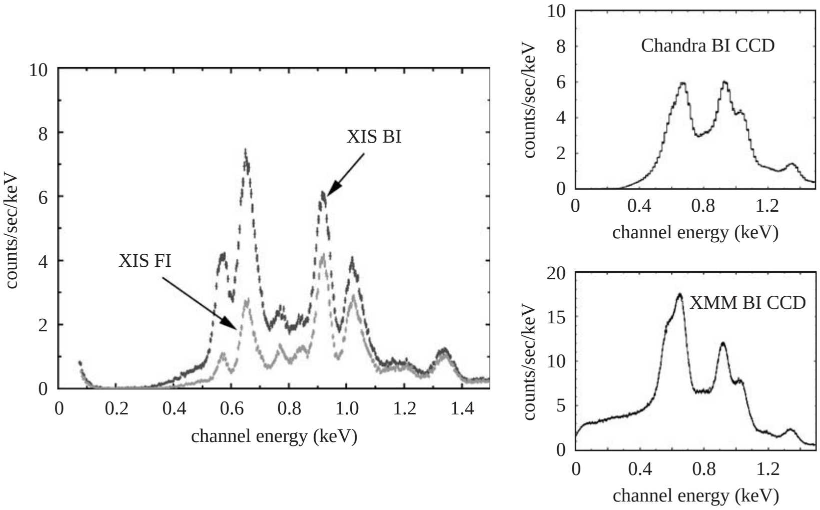

Fig. 4. Simulated spectrum of the supernova remnant E0102-72.3: XIS (left), *Chandra* BI (right upper) and XMM BI (right lower).

to read out all pixels, if neither the Window nor the Burst options (see below) are specified. In the P-sum mode, the pixel data from multiple rows are summed in the Y-direction on the CCD, and the summed data are put in the Pixel RAM as a single row. The number of the summed rows is selected from 64, 128, and 256. The P-sum mode has no spatial resolution in the Y-direction, but the time resolution is significantly improved to $8\,\mathrm{s}/1024$–7.8 ms.

Two options are available for the Normal mode: Burst and Window options. In the Burst option, the exposure time can be chosen arbitrarily within the read-out interval (8 s). This option may be used to avoid pileup. If an exposure time of t's is chosen, however, a dead time of $8 - t$'s cannot be avoided during each read-out interval. In the Window option, only a part of the imaging area within a certain range of Y-direction is read out. The window width is selected from among 64, 128, and 256 rows. This option may also be used to reduce an exposure time to avoid pileup. The Burst and Window options may be used simultaneously.

Editing modes describe how detected events are handled. Three modes are available for the Normal mode: 5×5, 3×3, and 2×2 modes. In the 5×5 mode, the position of a detected event and all pulse heights of 5×5 pixels centered at the event are sent to the telemetry. In the 3×3 mode, the event position and the pulse heights of 3×3 pixels centered at the event are sent to the telemetry. Moreover, the 16-bit information of the surrounding 16 pixels is sent out, which describes which pixels have a pulse height larger than the outer split threshold. The total pulse height of those exceeding the threshold among the 16 pixels is also sent to the telemetry. In the 2×2 mode, the event position and the pulse heights of 2×2 pixels including the event center and the second highest pixel are sent to the telemetry. The position of the 2×2 pixels in the 3×3 pixels is also output. Moreover, the 8-bit information of the eight pixels out of the 12 surrounding pixels excluding the corner four pixels is sent to the telemetry, which contains information on which pixels have a pulse height larger than the outer split threshold. The 5×5 or 3×3 mode is usually used whenever it is possible within the telemetry limit.

For the P-sum mode, only the Timing mode is available. The pulse height, position, and grade of the event are output, where the grade describes how the event is split into the adjacent pixels. The total pulse height calculated according to the grade is also sent to the telemetry.

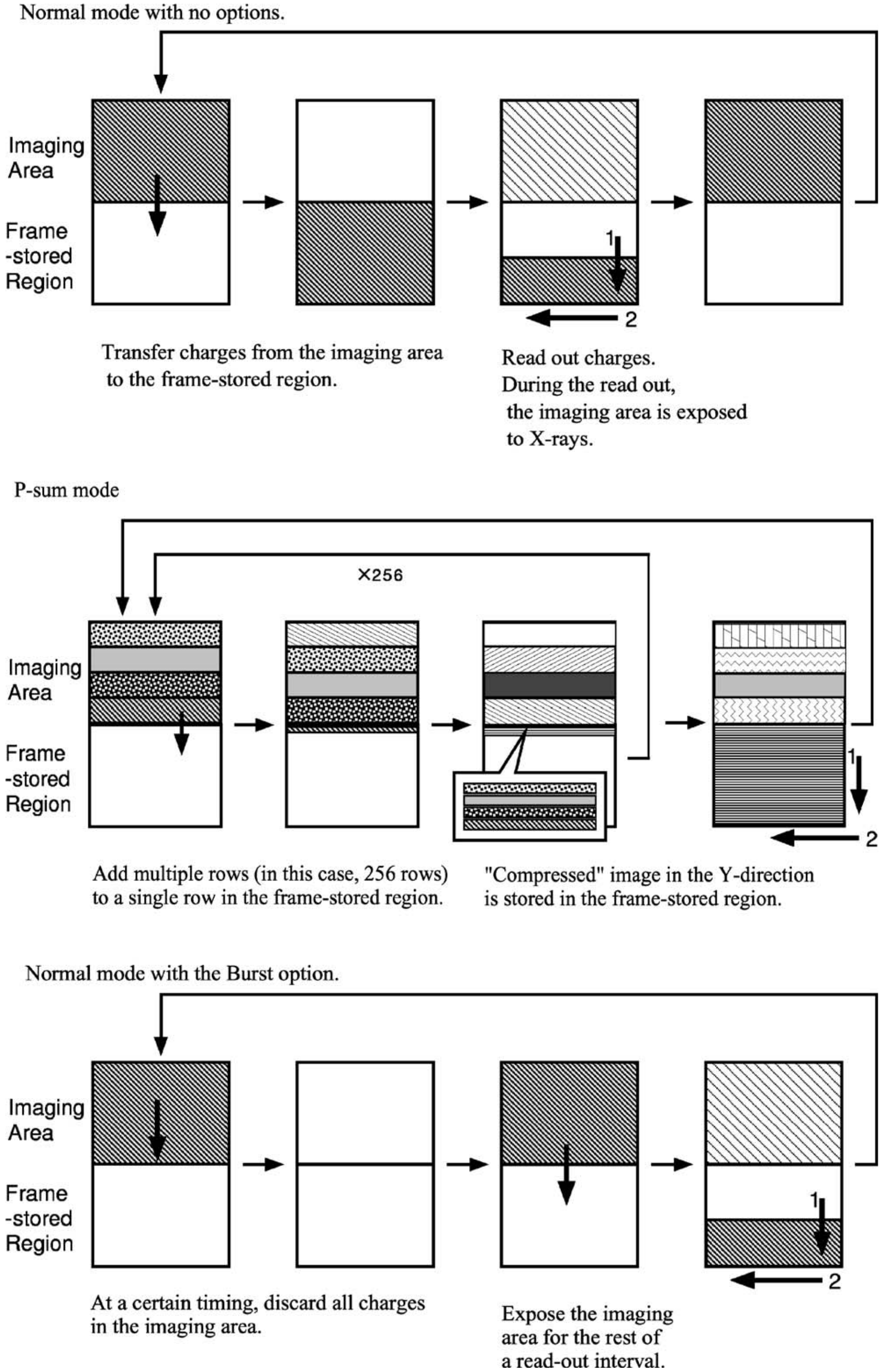

Fig. 5. Schematic views of the Normal mode (top), the P-sum mode (middle), and the Normal mode with the Burst option (bottom).

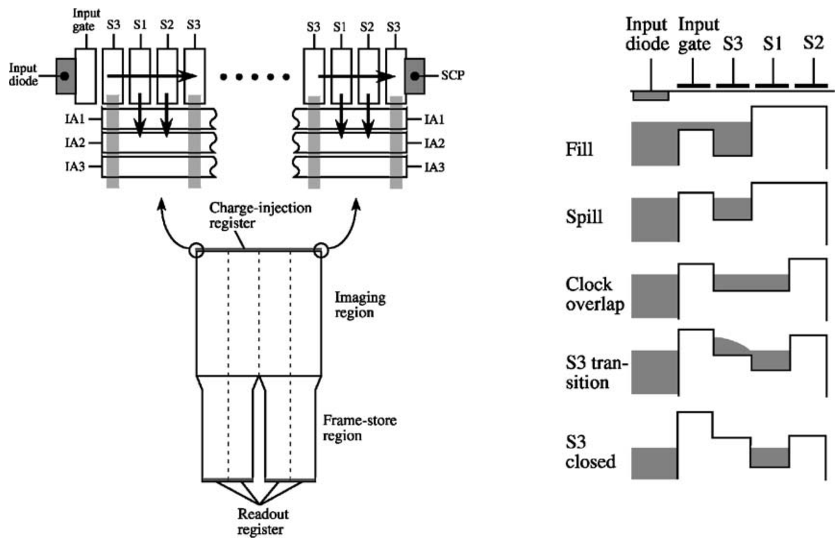

Fig. 6. Schematic view of charge injection: (left) the serial register for charge injection, and (right) the fill and spill method for charge injection. IA1–3 and S1–3 are the names of the electrodes.

5. Charge injection

The XIS of Astro-E2 is equipped with a charge injection capability, which is one of the new characteristics compared with the XIS for the lost Astro-E satellite [7,10]. Any amount of charge can be injected into the CCD pixels. By comparing the input charge and the read-out charge, the charge transfer efficiency (CTE) can be measured for each column of the CCD.

A serial register is equipped on the top of the imaging area for the charge injection (Fig. 6). The "fill and spill" method is used to input the charge. When the input gate is pulled up to a high level, electrons flow into the S3 ("fill"). The input gate then returns to a low level, and a certain amount of charge is left at the S3 ("spill"). We can control the amount of charge by adjusting the difference of voltage between the input gate and S3. The injected charge is transferred by the serial clock and put into a pixel at the top of the imaging area.

6. Radiation damage

The performance of the X-ray CCDs degrades gradually due to radiation damage by cosmic rays. This results in an increase of the dark current and a decrease of the CTE. We operate the XIS at $-90\,^{\circ}\mathrm{C}$ in order to minimize the effect of the increase of the dark current. We can correct the degradation of the CTE by measuring the CTE regularly with the ^{55}Fe sources and the charge injection function.

The degradation of the CTE is caused by charge traps in the CCDs produced by cosmic rays. When a charge packet encounters an empty trap, some electrons in the packet are captured in the trap. If a trap is already filled, however, the packet will not lose electrons. We can recover the degradation of the CTE by injecting charges (referred to as "sacrifice events") to fill traps before transferring charge packets produced by X-rays from celestial objects [11].

7. Summary

We have reviewed the X-ray CCD cameras on board Astro-E2, which are known as the X-ray Imaging Spectrometers (XISs). Compared with the other two detectors (XRS and HXD) on board Astro-E2, the XIS is the only instrument having an imaging capability. The XIS also has moderate energy resolution. Both the FI and BI CCDs are utilized in the XIS. The BI CCD of the XIS has nearly the same energy resolution as that of the FI CCDs, which is quite different from the BI CCDs on board *Chandra* and *XMM-Newton*. The XIS further has the capability of charge injection. This function is useful in measuring the CTE for each column of the CCD.

Acknowledgements

We would like to express our thanks to Mr. Chris Baluta for his careful review of the manuscript. This work is supported by a Grant-in-Aid for the 21st Century COE "Center for Diversity and Universality in Physics". HM is also supported by a Grant-in-Aid for scientific research 15740119 from Japan Society for the Promotion of Science.

References

[1] B.E. Burke, et al., IEEE Trans. ED-46 (1991) 1069.
[2] M.C. Weisskopf, et al., Publ. Astron. Soc. Pacific 114 (2002) 1.
[3] D.H. Lumb, et al., Proc. SPIE 4140 (2000) 22.
[4] K. Mitsuda, et al., ASP Conf. Ser. 251 (2001) 570.
[5] K. Makishima, et al., ASP Conf. Ser. 251 (2001) 564.
[6] M.W. Bautz, et al., Proc. SPIE 5501 (2004) 111.
[7] H. Nakajima et al., Nucl. Instr. and Meth. A (2005), this Volume.
[8] B. LaMarr, et al., Proc. SPIE 5501 (2004) 385.
[9] B.E. Burke, M. Lesser, IEEE Nucl. Symp. 51 (2004) 2322.
[10] G.Y. Prigozhin, et al., Proc. SPIE 5501 (2004), in press.
[11] K.C. Gendreau, Ph.D. Thesis, Massachusetts Institute of Technology, 1005.